Biomedical Optics EXPRESS

Optically investigating Nd^{3+}-Yb^{3+} cascade sensitized upconversion nanoparticles for high resolution, rapid scanning, deep and damage-free bio-imaging

Yuxiang Zhao,[1] Qiuqiang Zhan,[1,*] Jing Liu,[1] and Sailing He[1,2,3]

[1]*SCNU-ZJU Joint Research Center of Photonics, South China Academy of Advanced Optoelectronics, South China Normal University (SCNU), 510006 Guangzhou, China*
[2]*Centre for Optical and Electromagnetic Research, State Key Laboratory of Modern Optical Instrumentations, Zhejiang University (ZJU), Hangzhou 310058, China*
[3]*Department of Electromagnetic Engineering, Royal Institute of Technology, 10044 Stockholm, Sweden*
[*]*qiuqiang.zhan@coer-scnu.org*

Abstract: The rapid development of upconversion nanoparticles (UCNPs) has been facing with a great challenge: intense emission, fast scanning, and deep imaging require high-power light irradiation with minimized heating effect (the intrinsic 975-nm excitation of Yb^{3+}-sensitized UCNPs have overheating problem). By shifting the excitation peak from 975 nm to 795 nm, Nd^{3+}-Yb^{3+} cascade sensitized upconversion nanoparticles (Nd-UCNPs) with minimized heating effect were reported as the new generation UCNPs. For the first time, within two optically modeled applications *in vitro* and *in vivo*, the damage outcomes under long time high power laser excitation were solidly calculated, complementing the damage-free study of Nd-UCNPs. The higher resolution (20% improvement) and five times faster scanning microscopy were successfully performed using Nd-UCNPs under safety laser power level. The computational results showed the Nd^{3+}-Yb^{3+} energy transfer efficiency would not compromise the deep imaging ability, and the red (650-nm) emission is worth to be enhanced for deep tissue imaging.

OCIS codes: (160.4236) Nanomaterials; (160.5690) Rare-earth-doped materials;

References and links

1. F. Auzel, "Upconversion and anti-stokes processes with f and d ions in solids," Chem. Rev. **104**(1), 139–174 (2004).
2. M. Haase and H. Schäfer, "Upconverting nanoparticles," Angew. Chem. Int. Ed. Engl. **50**(26), 5808–5829 (2011).
3. C. T. Xu, N. Svensson, J. Axelsson, P. Svenmarker, G. Somesfalean, G. Chen, H. Liang, H. Liu, Z. Zhang, and S. Andersson-Engels, "Autofluorescence insensitive imaging using upconverting nanocrystals in scattering media," Appl. Phys. Lett. **93**(17), 171103 (2008).
4. L. Caillat, B. Hajj, V. Shynkar, L. Michely, D. Chauvat, J. Zyss, and F. Pellé, "Multiphoton upconversion in rare earth doped nanocrystals for sub-diffractive microscopy," Appl. Phys. Lett. **102**(14), 143114 (2013).
5. G. Chen, J. Shen, T. Y. Ohulchanskyy, N. J. Patel, A. Kutikov, Z. Li, J. Song, R. K. Pandey, H. Ågren, P. N. Prasad, and G. Han, "(α-NaYbF4:Tm3+)/CaF2 Core/Shell Nanoparticles with Efficient Near-Infrared to Near-Infrared Upconversion for High-Contrast Deep Tissue Bioimaging," ACS Nano **6**(9), 8280–8287 (2012).
6. J. Zhou, Z. Liu, and F. Li, "Upconversion nanophosphors for small-animal imaging," Chem. Soc. Rev. **41**(3), 1323–1349 (2012).
7. Y. I. Park, K. T. Lee, Y. D. Suh, and T. Hyeon, "Upconverting nanoparticles: a versatile platform for wide-field two-photon microscopy and multi-modal in vivo imaging," Chem. Soc. Rev. **2014**, 1039 (2014).
8. Y. Liu, D. Tu, H. Zhu, and X. Chen, "Lanthanide-doped luminescent nanoprobes: controlled synthesis, optical spectroscopy, and bioapplications," Chem. Soc. Rev. **42**(16), 6924–6958 (2013).
9. G. Chen, H. Qiu, P. N. Prasad, and X. Chen, "Upconversion nanoparticles: design, nanochemistry, and applications in theranostics," Chem. Rev. **114**(10), 5161–5214 (2014).
10. C. T. Xu, Q. Zhan, H. Liu, G. Somesfalean, J. Qian, S. He, and S. Andersson-Engels, "Upconverting nanoparticles for pre-clinical diffuse optical imaging, microscopy and sensing: Current trends and future challenges," Laser Photon. Rev. **7**(5), 663–697 (2013).

#227211 - $15.00 USD Received 4 Dec 2014; revised 27 Jan 2015; accepted 6 Feb 2015; published 18 Feb 2015

11. Q. Zhan, J. Qian, H. Liang, G. Somesfalean, D. Wang, S. He, Z. Zhang, and S. Andersson-Engels, "Using 915 nm Laser Excited $Tm^{3+}/Er^{3+}/Ho^{3+}$- Doped NaYbF4 Upconversion Nanoparticles for in Vitro and Deeper in Vivo Bioimaging without Overheating Irradiation," ACS Nano **5**(5), 3744–3757 (2011).
12. Q. Zhan, S. He, J. Qian, H. Cheng, and F. Cai, "Optimization of optical excitation of upconversion nanoparticles for rapid microscopy and deeper tissue imaging with higher quantum yield," Theranostics **3**(5), 306–316 (2013).
13. H. Liu, C. T. Xu, G. Dumlupinar, O. B. Jensen, P. E. Andersen, and S. Andersson-Engels, "Deep tissue optical imaging of upconverting nanoparticles enabled by exploiting higher intrinsic quantum yield through use of millisecond single pulse excitation with high peak power," Nanoscale **5**(20), 10034–10040 (2013).
14. W. Feng, X. Zhu, and F. Li, "Recent advances in the optimization and functionalization of upconversion nanomaterials for in vivo bioapplications," NPG Asia Materials **5**(12), e75 (2013).
15. Z. Gu, L. Yan, G. Tian, S. Li, Z. Chai, and Y. Zhao, "Recent advances in design and fabrication of upconversion nanoparticles and their safe theranostic applications," Adv. Mater. **25**(28), 3758–3779 (2013).
16. J. Zhao, D. Jin, E. P. Schartner, Y. Lu, Y. Liu, A. V. Zvyagin, L. Zhang, J. M. Dawes, P. Xi, J. A. Piper, E. M. Goldys, and T. M. Monro, "Single-nanocrystal sensitivity achieved by enhanced upconversion luminescence," Nat. Nanotechnol. **8**(10), 729–734 (2013).
17. J. Shen, G. Chen, A.-M. Vu, W. Fan, O. S. Bilsel, C.-C. Chang, and G. Han, "Engineering the Upconversion Nanoparticle Excitation Wavelength: Cascade Sensitization of Tri-doped Upconversion Colloidal Nanoparticles at 800 nm," Adv. Opt. Mater. **1**(9), 644–650 (2013).
18. Y.-F. Wang, G.-Y. Liu, L.-D. Sun, J.-W. Xiao, J.-C. Zhou, and C.-H. Yan, "Nd3+-Sensitized Upconversion Nanophosphors: Efficient in Vivo Bioimaging Probes with Minimized Heating Effect," ACS Nano **7**(8), 7200–7206 (2013).
19. X. Xie, N. Gao, R. Deng, Q. Sun, Q.-H. Xu, and X. Liu, "Mechanistic Investigation of Photon Upconversion in Nd3+-Sensitized Core-Shell Nanoparticles," J. Am. Chem. Soc. **135**(34), 12608–12611 (2013).
20. Y. Zhong, G. Tian, Z. Gu, Y. Yang, L. Gu, Y. Zhao, Y. Ma, and J. Yao, "Elimination of photon quenching by a transition layer to fabricate a quenching-shield sandwich structure for 800 nm excited upconversion luminescence of Nd3+-sensitized nanoparticles," Adv. Mater. **26**, 2831–2837 (2014).
21. X. Li, R. Wang, F. Zhang, L. Zhou, D. Shen, C. Yao, and D. Zhao, "Nd3+ Sensitized Up/Down Converting Dual-Mode Nanomaterials for Efficient In-vitro and In-vivo Bioimaging Excited at 800 nm," Sci. Rep. **3**, 3536 (2013).0
22. G. Alexandrakis, F. R. Rannou, and A. F. Chatziioannou, "Tomographic bioluminescence imaging by use of a combined optical-PET (OPET) system: a computer simulation feasibility study," Phys. Med. Biol. **50**(17), 4225–4241 (2005).
23. C. T. Xu, P. Svenmarker, H. Liu, X. Wu, M. E. Messing, L. R. Wallenberg, and S. Andersson-Engels, "High-Resolution Fluorescence Diffuse Optical Tomography Developed with Nonlinear Upconverting Nanoparticles," ACS Nano **6**(6), 4788–4795 (2012).
24. F. C. Henriques, Jr., "Studies of thermal injury; the predictability and the significance of thermally induced rate processes leading to irreversible epidermal injury," Arch. Pathol. (Chic) **43**(5), 489–502 (1947).
25. M. N. Rylander, Y. Feng, R. Jason Stafford, K. R. Diller, A. Volgin, Y. Zhang, J. Bass, and J. D. Hazle, "Optimizing heat shock protein expression induced by prostate cancer laser therapy through predictive computational models," J. Biomed. Opt. **11**, 041113 (2006).
26. M. L. Cohen, "Measurement of the thermal properties of human skin. areview," J. Invest. Dermatol. **69**(3), 333–338 (1977).
27. C. T. Xu, J. Axelsson, and S. Andersson-Engels, "Fluorescence diffuse optical tomography using upconverting nanoparticles," Appl. Phys. Lett. **94**(25), 251107 (2009).
28. M. Keijzer, W. M. Star, and P. R. M. Storchi, "Optical diffusion in layered media," Appl. Opt. **27**(9), 1820–1824 (1988).
29. H. Ding, J. Q. Lu, W. A. Wooden, P. J. Kragel, and X. H. Hu, "Refractive indices of human skin tissues at eight wavelengths and estimated dispersion relations between 300 and 1600 nm," Phys. Med. Biol. **51**(6), 1479–1489 (2006).
30. H. H. Pennes, "Analysis of tissue and arterial blood temperatures in the resting human forearm," J. Appl. Physiol. **1**(2), 93–122 (1948).
31. M. N. Rylander, Y. Feng, J. Bass, and K. R. Diller, "Heat shock protein expression and injury optimization for laser therapy design," Lasers Surg. Med. **39**(9), 731–746 (2007).
32. W. R. Zipfel, R. M. Williams, and W. W. Webb, "Nonlinear magic: multiphoton microscopy in the biosciences," Nat. Biotechnol. **21**(11), 1369–1377 (2003).
33. J. Pichaandi, J.-C. Boyer, K. R. Delaney, and F. C. Van Veggel, "Two-photon upconversion laser (scanning and wide-field) microscopy using Ln3+-doped NaYF4 upconverting nanocrystals: a critical evaluation of their performance and potential in bioimaging," J. Phys. Chem. C **115**(39), 19054–19064 (2011).
34. E. C. Halperin, L. W. Brady, D. E. Wazer, and C. A. Perez, *Perez & Brady's Principles and Practice of Radiation Oncology* (Lippincott Williams & Wilkins, 2013).

1. Introduction

Lanthanide-doped upconversion nanoparticles (UCNPs) can absorb multiple near infrared photons via intermediate energy states and convert into one short wavelength photon [1, 2]. Superior to the conventional synthetic dyes and quantum dots, UCNPs enable nonbleaching, nonblinking, autofluorescence-free, deep and high resolution bioimaging with narrow-band anti-stoke upconverting (UC) emission under continuous wave (CW)

#227211 - $15.00 USD Received 4 Dec 2014; revised 27 Jan 2015; accepted 6 Feb 2015; published 18 Feb 2015

light irradiation [3–5]. Due to these advantages, UCNPs have been widely employed in bioimaging, diffusion optical tomography, bio-sensing and photodynamic therapy [6–10]. However, the most commonly studied Yb^{3+}-sensitized UCNPs (Yb-UCNPs) have exhibited the weakness that the intrinsic strong absorption of water at 975 nm (the peak excitation of Yb^{3+}) would induce overheating effect and impair penetration depth in the biospecimen [11].

One way to suppress the heating effect is decreasing the excitation power by enhancing the quantum yield (QY). In previous work, we proposed the doubled QY using the pulsed light [12]. Liu et al experimentally validated the feasibility of QY enhancement with the microsecond pulsed laser [13]. Besides, various chemical optimizations were reported [14, 15], and recently the significant enhancement by a factor of 70 was achieved by high excitation irradiance combined with high activator concentration [16].

However, the QY of UC emission is intrinsically low due to the nonlinear mechanism and hard to make great improvement. Focus has been shifted to another approach-engineering the excitation wavelength. Specifically, an alternative 915 nm laser was selected for Yb-UCNPs imaging to diminish the overheating effect and increase the penetrating depth [11]. More recently, Nd^{3+} was introduced to UCNPs as the new sensitizer because of its strong absorption band around 795 nm, which would induce the minimized heating effect in bio-system [17, 18]. Subsequently, the highly efficient cascade energy transfer (ET) process ($Nd^{3+}\rightarrow Yb^{3+}\rightarrow Ln^{3+}$) were achieved by modulating the core-shell structure and doping concentration [19, 20]. Meanwhile, potential deep imaging ability of this novel UCNPs were indicated [18, 20, 21].

Thanks to the minimized heating effect and improved penetrability of 795-nm-light, Nd^{3+}-Yb^{3+} cascade sensitized upconversion nanoparticles (Nd-UCNPs) have been regarded as the new generation of UCNPs. However, the study of this novel UCNP is still in the early stage. In this work, we investigated many facets of Nd-UCNPs to propose some potential advantages as well as points to note in the bioimaging. Firstly, using two bioimaging models *in vitro* and *in vivo*, the damage effects of biosamples were firstly simulated for a long period and substantially indicated the damage-free imaging of Nd-UCNPs. The higher resolution Nd-UCNP (20% improvement) was realized with 795-nm-laser excitation and higher safety power of Nd-UCNPs induced five times faster scanning microscopy using 795-nm-laser. Furthermore, the investigation of multi-step UC process is not sufficient with respect to the deep imaging ability. The limited Nd^{3+}-Yb^{3+} ET efficiency may reduce the excitation energy and partly decrease the imaging depth. For the first time, we calculated its impact on the imaging depth and clearly demonstrated that the Nd-UCNPs with only 13% ET efficiency have better deep imaging ability than the Yb-UCNPs. In addition, it is notable that the strong green/blue emissions of current Nd-UCNPs would also affect the imaging depth due to its larger scattering and absorption than the red or the NIR emission in tissue. The simulating results confirmed the necessity of shifting the strong emission range of Nd-UCNPs from the green/blue to the red band.

2. Methods

2.1 Experiments

As shown in Fig. 1(a), the classic dual-doped $NaYF_4$: 30%Yb, 0.5%Er/ $NaYF_4$ and the novel tri-doped $NaYF_4$: 30%Yb, 0.5%Er, 1%Nd/ $NaYF_4$: 20%Nd core/shell UCNPs with the same Yb^{3+} and Er^{3+} doping concentration, synthesized through the recently reported protocols [19], were used as the representative of Yb-UCNPs and Nd-UCNPs for the *in vitro* high resolution and rapid scanning microscopy experiments. The nanoparticles, with the size of about 20 nm, were characterized using transmission electronic microscopy and absorption spectra under the same sample concentration. Two quasi CW laser beam of 795-nm and 975-nm from a tunable Ti: Sapphire laser (Mira HP, Coherent) were optimized and then coupled into the microscopy as the excitation sources. The emission spectrum was collected by a compact spectrometer (QE65000, Ocean Optics). The imaging experiments were implemented on a multiphoton laser scanning microscope system (MPE1000, Olympus). The lifetime data were measured with a time-correlated single photon counting system (Nanoharp300, PicoQuant).

#227211 - $15.00 USD Received 4 Dec 2014; revised 27 Jan 2015; accepted 6 Feb 2015; published 18 Feb 2015

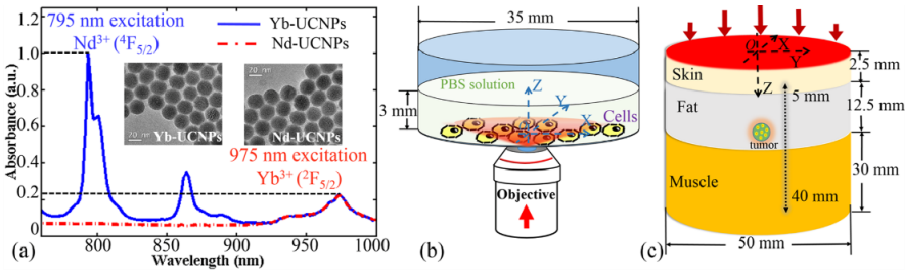

Fig. 1. (a) Normalized absorption spectra and TEM images of $NaYF_4$: 30%Yb, 0.5%Er/ $NaYF_4$ nanoparticles (Yb-UCNPs) and $NaYF_4$: 30%Yb, 0.5%Er, 1%Nd/ $NaYF_4$: 20%Nd nanoparticles (Nd-UCNPs). Schematics of (b) cell-in-celldish model and (c) three-layer pork tissue model.

2.2 Simulating models

Imaging model

In order to investigate the damage distributions and the deep imaging upconverting process of Nd-UCNPs, cell-in-celldish model *in vitro* and three-layer pork tissue model *in vivo* were constructed.

Cell-in-celldish model. As shown in Fig. 1(b), we set up a celldish model (cells incubation environment: 37°C and 5% CO_2) which contains a 3-mm-thick cylinder area (radius: 17.5 mm) for the 3 mL phosphate buffer solution (PBS), while 18000 UCNP-labeled cells are adherent on the bottom. This model is implemented on an inverted microscopy with CW laser beam focused by a commonly used oil-immersed objective (NA = 1.35) in microscopy imaging of UCNPs. The same excitation power 100 mW of two different wavelengths were used in this model (focal power density: 1.64×10^5 W/m^2 of 975 nm laser; 2.467×10^5 W/m^2 of 795 nm laser). The Rayleigh length (Z_R = 605 nm and 493 nm, for 975 nm and 795 nm light) of the focused beam obtained from the equation $Z_R = \pi\omega_0^2 / \lambda$ is so small that the volume of the laser beam transmitted conical area in PBS can be can be approximately obtained: $V = \pi hR^2 / 3 = 120.5\times10^{-9}\, m^3$.

Pork tissue model. To make the model more factual, a three-layer pork tissue model with similar optical properties with human tissue was modeled as shown in Fig. 1(c). The cylindrical tissue bearing a UCNP-labeled malignant tumor is irradiated by a circular CW laser beam (radius: 25 mm, power density: 500 mW/cm^2). The depth of tumor is defined as the distance from the surface center to the tumor center and varies from 5 mm to 40 mm.

Theoretical model

The heat transfer equation and the cell/tissue damage model were built to simulate the spatiotemporal temperature and damage distributions. The diffusion equation was used to investigate the imaging depth in tissue imaging. The detailed parameters and boundary conditions settings involved in these models were determined according to tissue optics, heat transfer and biological damage [11, 12, 22–26].

Diffusion equation. The light propagating in turbid media can be approximately modeled using diffusion equation ($\mu_s >> \mu_a$). The fluorescence diffusion imaging in the biological tissue can be described as two diffusion equations: one is for the excitation propagation (Eq. (1)) and the other is for the fluorescence propagation (Eq. (2) and (3)). In the steady state, we can describe them as [27]:

$$(\mu_a^{ex} - D^{ex}\nabla^2)\varphi^{ex}(r) = S(r) \tag{1}$$

$$(\mu_a^{em} - D^{em}\nabla^2)\varphi^{em}(r) = \eta\mu^{ex}[\varphi^{ex}(r)]^2 \tag{2}$$

$$(\mu_a^{em} - D^{em}\nabla^2)\varphi^{em}(r) = \eta\mu^{ex}[Y\varphi^{ex}(r)]^2 \tag{3}$$

#227211 - $15.00 USD Received 4 Dec 2014; revised 27 Jan 2015; accepted 6 Feb 2015; published 18 Feb 2015

where $D^{ex\backslash em} = 1/3(\mu_a^{em\backslash ex} + \mu_s^{'em\backslash ex})$, and μ_a, $\mu_s^{'}$ is the diffusion coefficient of excitation or emission light, the absorption coefficient, and the reduced scattering coefficient, $\varphi^{ex\backslash em}$ the photon fluence rate of excitation or emission light, *Y* the energy transfer efficiency from Nd^{3+} to Yb^{3+} [17], S(r) the source term that set in the position of $(0,0,1/\mu_s^{'})$, η the power-related QY coefficient calculated from the reported work [23], and μ_{ex} the absorption coefficient of excitation wavelength for UCNPs (here we set 5 times larger absorbance of Nd-UCNPs at 795 nm than Yb-UCNPs at 975 nm as indicated in Fig. 1(a)). The parameters are listed in Table 1.

For the skin-air interface, the Neumann boundary condition was used to account for the refractive index mismatch between tissue (n_{tissue}~1.4) and air (n_{air}~1) [28, 29]: $n(D\nabla\varphi(r,t)) + \varphi(r,t)/2A = 0$. Here A = 2.74 in this model. For the other parts, we used the continuous boundary conditions (the modeled area is a part of whole tissue).

Table 1. Diffusion fluorescence model parameters in pork tissue model [11, 12, 22, 23]

	795 nm	975 nm	540 nm	650 nm	800 nm
μ_a(skin)	0.0143	0.2452	0.1554	0.0117	0.0137
μ_a(fat)	0.0119	0.2435	0.0089	0.0028	0.0114
μ_a(muscle)	0.0148	0.2454	0.1800	0.0139	0.0141
μ_s'(skin)	18.3840	14.6872	28.1327	22.9425	18.2577
μ_s'(fat)	11.0303	9.8995	13.5399	12.2727	10.9938
μ_s'(muscle)	2.6487	1.4896	7.8833	4.6735	2.6022
μ_a(tumor@fat)	0.1504	0.6136	-	-	-
μ_a(tumor@muscle)	0.1562	0.6174	-	-	-
μ_s'(tumor@fat)	11.582	10.3948	14.2169	12.8860	11.5435
μ_s'(tumor@muscle)	2.7811	1.5640	8.2775	4.9100	2.7323
μ^{ex}(UCNPs)	0.6330	0.1266	-	-	-
η	0.00000175	0.00000175	0.00000175	0.00000175	0.00000175

Heat Transfer Equation. The spatiotemporal temperature distributions can be modeled and predicted using the Pennes's bioheat transfer equation [30, 31]:

$$\rho c(dT/dt) = \nabla(k\nabla T) + Q \tag{4}$$

where T(K) is the solution temperature, t(s) the time, ρ, c and k the density, heat capacity and thermal conductivity of PBS solution or relevant tissue part, and Q the heat source. The parameters are listed in Table 2 and 3.

A heat flux condition combined with Newton's cooling law was used as the boundary condition to describe a convection process as: $K(dT/dn) = h(T - T_0)$, where h is the overall heat transfer coefficient for the region adjacent to the model boundary. For the cell incubation system, the internal temperature $T(t_0)$ = 37°C, and typical values h_{air} = 25 W/(m^2·K), and h_{wall} = 5 W/(m^2·K) were used. For the pork tissue model, the external temperature $T(t_0)$ = 23°C, typical values hair = 25 W/(m^2·K) was used. We set $T(t_0)$ = 34°C for the skin and $T(t_0)$ = 37°C for the fat and muscle. The internal interfaces here between 3 layers were considered as continuous.

Cell damage model. The Arrhenius injury model was used to predict the cell and tissue injury in the process of *in vivo* and *in vitro* bioimaging. The cell/tissue damage rate can be calculated as [24, 31]:

$$k = Ae^{-Ea/(RT)} \tag{5}$$

where Ea is the activation energy, R the universal gas constant, T the transient temperature, and A scaling factor. The parameters are listed in Table 2 and 3. The cells/tissue that are damaged over time is given by the normalized damage index:

$$F_D = 1 - e^{-\int kdt} \tag{6}$$

Here it is defined that the cell/tissue is damaged when $F_D \geq 0.6$ [25].

#227211 - $15.00 USD Received 4 Dec 2014; revised 27 Jan 2015; accepted 6 Feb 2015; published 18 Feb 2015

Table 2. Heat transfer and cell damage model parameters in Cell-in-Celldish model [11, 25]

Parameter	Value
ρ	1000 kg/m^3
c	4200 J/(Kg·K)
k	0.58 W(m·K)
T(t_0)	310.15 K
Q(795)	5850 W/m^3
Q(975)	112880 W/m^3
A	1.8×10^{36} $s^{(-1)}$
Ea	2.38×10^5 KJ/mol
R	8.3145 J/mol·K

Table 3. Heat transfer and tissue damage model parameters in Pork Tissue model [24, 26]

	p (Kg/m^3)	c (J(Kg·K))	K (W(m·K))	T(t_0) (K)	A (s^{-1})	Ea (KJ/mol)	R (J/mol·K)
skin	1020	3350	0.29	307.15			
fat	895	2300	0.195	310.15	3.1×10^{98}	6.3×10^5	8.3145
muscle	1030	3700	0.46	310.15			

3. Results and discussion

High-resolution microscopy. It is valuable that multiphoton microscopy under CW laser excitation could be implemented due to the high nonlinearity of UCNPs. However, traditional 975 nm excitation compromise the resolution using relative long excitation wavelength according to the equation [32]:

$$\Delta x \setminus \Delta y \approx 1.22\lambda / 2\mathrm{NA}(n)^{1/2} \tag{7}$$

where λ is the excitation wavelength, NA the numerical aperture of the objective, and n the n-photon process. According to Eq. (7), shorter wavelength 795 nm excitation will provide higher resolution.

In this study, the imaging sample was prepared by spin-coating Nd-UCNPs highly dispersed in chloroform on the coverslips. The incident beam was focused by a 1.00 NA objective (no objective with 1.35NA available in our laboratory). The green emission (two-photon) of Er^{3+}-doped UCNPs was detected. The exciting power was below the saturation level in view of the multiphoton process. Two images of the same UCNP spot were collected by using 795-nm-laser and 975-nm-laser, respectively. The images and the FWHMs analysis by fitting the emission profiles are shown in Fig. 2. Experimental FWHMs of 795 nm and 975 nm excitation were calculated as the value of 345 nm and 425 nm, respectively, in good agreement with the theoretical values (342 nm and 420 nm). We found that the FWHM in the case of 795 nm excitation is 20% smaller than that of the 975 nm excitation. Extending this investigation to the 3D microscopy, the excitation of 795-nm light can also lead to the 20% improvement of z-axis resolution, theoretically revealing better optical sectioning ability. After calculating according to $V = 4\pi\Delta x\Delta y\Delta z / 3$, 795-nm light can reduce the focal volume at half. This investigation suggested that the higher resolution of Nd-UCNPs should be appreciated and explored in multiphoton imaging using low-cost 795-nm CW laser as excitation.

#227211 - $15.00 USD Received 4 Dec 2014; revised 27 Jan 2015; accepted 6 Feb 2015; published 18 Feb 2015

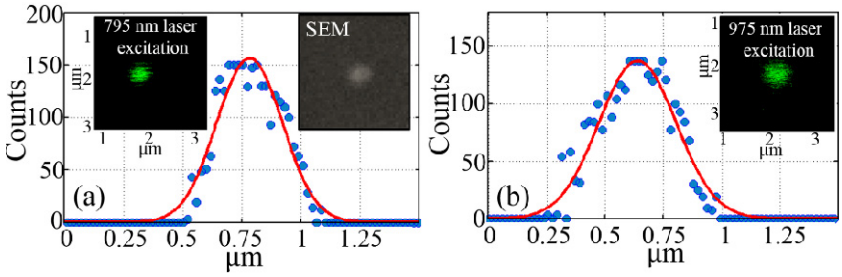

Fig. 2. Multiphoton imaging of (a) 795-nm-excited UCNP (Inset: the SEM image of single UCNP on the coverslip) and (b) 975-nm-excited UCNP.

Damage-free microscopy *in vitro*. The minimized heating effect of 795 nm laser have been simply demonstrated in the cell imaging [18]. However, for the live cell study it is imperative to quantify the damage effect of samples during the *in vitro* imaging process. 20 mins irradiation was simulated combined with the same power 100 mW of two different wavelengths (focal power density: 1.64×10^5 W/m^2 of 975 nm laser; 2.467×10^5 W/m^2 of 795 nm laser) to investigate the spatiotemporal temperature and damage outcomes of cell lines. In the common microscopy, the imaging process probably has to last for long time (*e.g.*, 20 mins) as we need to adjust the focal plane, search the region of interest, set the system configurations and collect the images (UCNPs has very long lifetime and the scanning is usually time-consuming [33], especially the optical tomography). The scanned area is very small and the focal point can be assumed as fixed here.

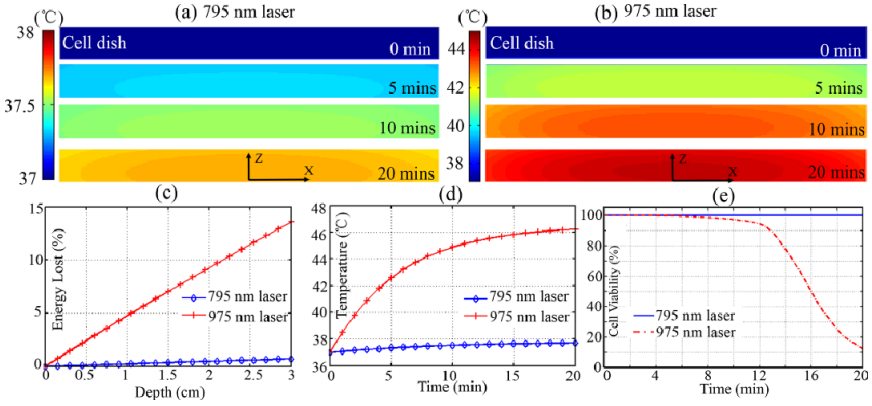

Fig. 3. Cross-section of the spatiotemporal temperature distributions of cell-in-celldish model under (a) 795 nm and (b) 975 nm laser excitation; (c) The laser energy lost in the 3-mm-thick PBS; (b) Time-resolved temperature variation of adhered cells (0, 0, 0.5 mm) in 20 min; (e) Cell viability prediction after 20 min excitation.

In the case of *in vitro* microscopy in Fig. 3 (a), the temperature of 795 nm excited whole cell system was relatively low and stable during 20 mins, whereas in Fig. 3 (b) the 975 nm laser apparently heated up the sample in 20 mins. In this model, we primarily concerned the temperature elevation for the adherent cells in Fig. 3(d). During the 5 mins, temperature of the celldish bottom didn't reach the apoptosis threshold under either 795 nm or 975 nm laser irradiation in Fig. 3(a), 3(b) and the cell lines kept healthy in Fig. 3(e). However, after 7 mins irradiation of 975 nm laser, the cell lines were heated up to 44 °C, higher than the hyperthermia temperature 42-43 °C, and this would probably induce severe cell apoptosis or damage in Fig. 3(e) [34]. This situation was getting much worse after longer time exposure of 975 nm laser, and even 90% of the cells were dead after 20 mins. On the contrary, almost all the cells under high power 795 nm laser excitation still survived after 20 mins in Fig. 3(e). This big difference could be reasoned that the heating effect was mainly due to the exciting energy absorption in cell dish. As shown in Fig. 3(c), less than 1% of 795 nm laser energy was lost after penetrating through 3-mm PBS solution layer, whereas the solution layer absorbed as much as about 15% energy of 975 nm laser. This

#227211 - $15.00 USD Received 4 Dec 2014; revised 27 Jan 2015; accepted 6 Feb 2015; published 18 Feb 2015

demonstration not only confirmed the damage-free *in vitro* imaging for Nd-UCNPs under high power excitation but also clearly indicated the quantified changing process of laser-induced transient heating and damage effect in a cell-in-celldish model.

Rapid scanning microscopy. The long lifetime and weak efficiency of UCNPs hindered its wide applications in fast-scanning microscopy because of the serious streak phenomenon as shown in Fig. 4(a). According to the simulating results in *in vitro* microscopy model, it enable higher power 795-nm laser irradiation for damage-free Nd-UCNP imaging. For the same UCNPs sample, the higher laser power excitation will induce shorter lifetime [16] and strong UC emission. This would greatly help to speed up the imaging scanning and keep the irradiating power below the safety level.

To keep both of the 795 nm and 975 nm excitation power at the same heat level for the bio-sample, 100mW (795-nm-laser focal power density: 2.467×10^5 W/m^2) and 5 mW (975-nm-laser focal power density: 0.82×10^4 W/m^2), which are much less laser power than that used in cell microscopy recently [21], were employed in view of the different absorption coefficients (0.0236 cm^{-1}@795 nm, about 20 times less than 0.4864 cm^{-1}@975 nm) of water. As indicated in Fig. 4(a) and 4(b), 5 mW 975 nm laser excitation introduced a scanning (2 μs/pixel) image with serious streaking phenomenon in which signal from one pixel disturbed the vicinity ones, while 100 mW 795 nm laser exhibited a better image quality with much shorter steak at the same speed (2 μs/pixel). After slowing down the scanning process in Fig. 4(c) and 4(d), we achieved high quality UC images at the speed of 40 μs/pixel for 975 nm laser and 8 μs/pixel for 795 nm laser, respectively. This evident difference can be explained by different lifetimes of two samples (30 μs for 5 mW 975 nm laser irradiation, 12.5μs for 100 mW 795 nm laser irradiation) in Fig. 4(e). This experiment has confirmed the rapid scanning ability of Nd-UCNPs under higher safety power level and would widely extend the UCNPs applications, such as multi-dimensional scanning microscopy, and fluorescence lifetime imaging microscopy.

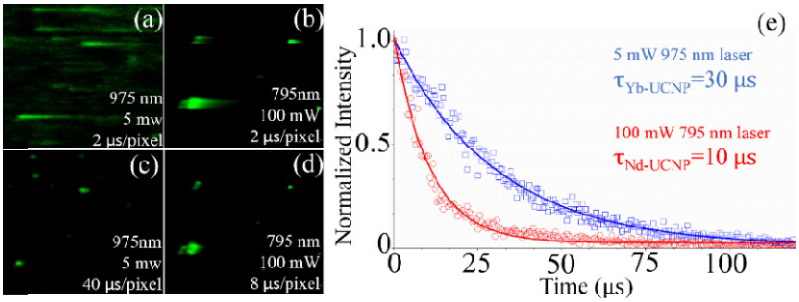

Fig. 4. Multiphoton scanning images of 975 nm excited Yb-UCNPs at (a) 2 μs/pixel, (c) 40 μs/pixel, and 795 nm excited Nd-UCNPs at (b) 2 μs/pixel and (d) 8 μs/pixel. (e) Lifetime measurements of two samples in (c) and (d).

Damage-free deep tissue imaging *in vivo*. The 795 nm laser induced minimized heating effect have been simply demonstrated only on the tissue surface [18, 20, 21]. However, it is also necessary to evaluate the damage outcomes inside tissue and complement the damage-free *in vivo* imaging study of Nd-UCNPs. In the simulation of *in vivo* imaging model, 10 mins irradiation combined with 500 mW/cm^2 CW laser were selected. It is well known that the irradiation time could be longer than several seconds in deep tissue imaging, as some preparations have to be made (*e.g.* positioning the imaging region of interest, adjusting the imaging lens and setting capture configurations) before capture. Therefore, 5 mins or even 10 mins laser irradiating is probably required for *in vivo* animal imaging, especially when performing the optical tomography and real-time monitoring. The absorbed laser energy will be converted into thermal energy and heated up the tissue. The fluence rate distribution of excitation laser were calculated in the tissue. As shown in Fig. 5(a)-5(c), due to high absorption much energy of the 975-nm laser was absorbed and heat up the tissue regionally. Specially, as shown in Fig. 5(e), a much higher temperature than the corresponding one at 0, 5, 10 min in Fig. 5(d). We also investigate the temperature and normalized damage index of two points at surface and inside tissue to

#227211 - $15.00 USD Received 4 Dec 2014; revised 27 Jan 2015; accepted 6 Feb 2015; published 18 Feb 2015

evaluate this difference. As shown in Fig. 5(f), the inner temperature is higher than the surface tissue in Fig. 5(f), which also indicates the inner tissue is damaged whereas the surface is still keep healthy after 6 mins in Fig. 5(i).

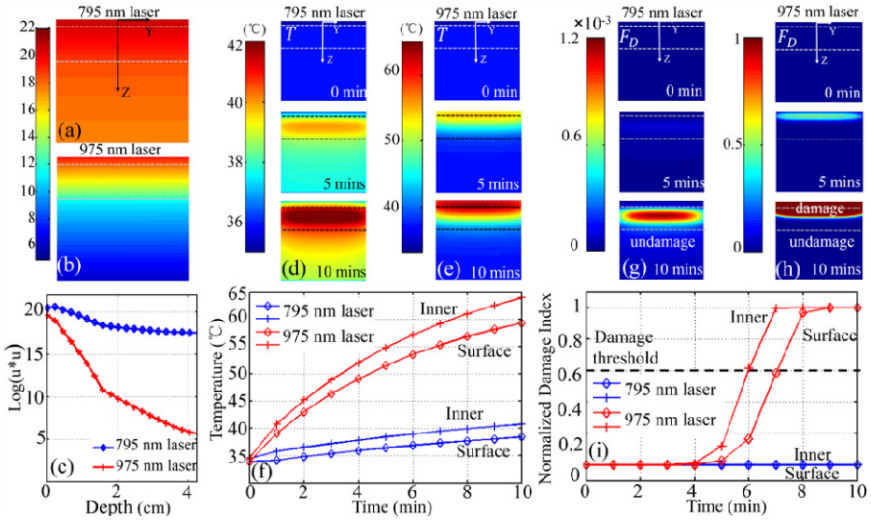

Fig. 5. Simulated distribution of the logarithm of square photon fluence rate ($\log(u^2)$) of (a) a 795 nm and (b) a 975 nm laser excitation; (c) ($\log(u^2)$) as a function of the tissue depth while the laser transmits light into the tissue model; Cross-section of the spatiotemporal temperature T distributions of 3-layer pork tissue model under (d) 795 nm and (e) 975 nm laser irradiation; (f) time-resolved temperature of surface (point (0, 0, 0 mm)) and inner (point (0, 0, 2 mm)) during 10 mins irradiation; Cross-section of the spatiotemporal normalized damage index F_D distributions under (g) 795 nm and (h) 975 nm laser irradiation. (i) time-resolved normalized damage index F_D of surface (point (0, 0, 0 mm)) and inner (point (0, 0, 2 mm)) during 10 mins of irradiation.

As shown in Fig. 5(e) and 5(h), after 5 mins 975 nm laser irradiation, the temperature in the area of skin and shallow fat rapidly increased to over 55 °C and these heated tissue began to get damaged. After 10 mins, the whole inner part of tissue was damaged as the temperature was beyond 60 °C. On the contrary in Fig. 5(d) and 5(g), the temperature of neither inner nor outer parts reached the hyperthermia temperature 42 °C under 795 nm laser irradiation and the whole tissue still kept healthy even after 10 mins. This simulation demonstrated the damage-free *in vivo* imaging inside tissue with Nd-UCNPs, and quantitatively showed the relationship of transient temperature and damage distribution in a pork tissue model.

The Impact of Nd^{3+}-Yb^{3+} ET efficiency (Y) on the imaging depth. Except the similar UC emission process in traditional Yb-UCNPs, there exist another three energy transfer processes of cascade multi-step sensitized Nd-UCNPs (e.g., Nd^{3+}, Yb^{3+}, Er^{3+} tri-doped UCNPs): the absorption of Nd^{3+}, the energy transfer from Nd^{3+} to Yb^{3+}, and the energy back-transfer from Er^{3+} to Nd^{3+}. All these three added processes would impact the integral UC efficiency in Fig. 6(a). However, thanks to the intrinsic intense absorbance of Nd^{3+} at 795 nm (Fig. 1(a)) and the elimination of energy back-transfer from activator to Nd^{3+} [20]. There is only the Nd^{3+}-Yb^{3+} ET efficiency that may badly affect the deep imaging ability. It is still unknown and necessary to study its impact on imaging depth when investigating the deep imaging ability of Nd-UCNPs.

The most currently reported Nd-UCNPs with strong 540-nm-emission [17, 18, 20, 21] were selected to calculate the impact of different ET efficiency on imaging depth. Meanwhile, the Yb-UCNPs with strong 800-nm-emission which have the largest imaging depth (≥3cm) [5] were studied as the comparison. Because of the different excitation and emission wavelength, exciting energy absorptivity and UC efficiency of two samples, it is not straightforward to distinguish which one enable the deeper tissue imaging.

#227211 - $15.00 USD Received 4 Dec 2014; revised 27 Jan 2015; accepted 6 Feb 2015; published 18 Feb 2015

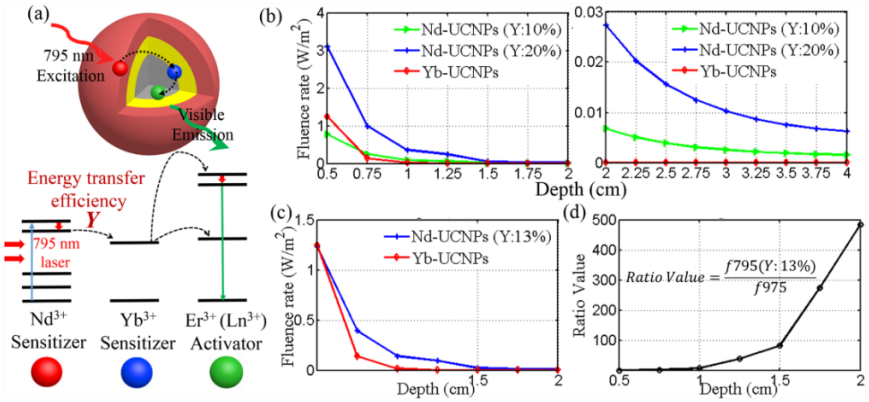

Fig. 6. (a) The schematic of cascade sensitizing process of Nd-UCNPs. (b) Simulated UC PL fluence rate at detecting point of Yb-UCNP emission and Nd-UCNP (Y: 10%, 20%) emission at different tumor depth (left: 0.5-2.0 cm; right: 2.0-4.0 cm). (c) UC PL fluence rate at detecting point of Yb-UCNP emission and Nd-UCNP (Y: 13%) emission and (d) the corresponding fluence rate ratio value of Nd-UCNP (Y:13%) emission and Yb-UCNP emission as a function of tumor depth (0.5-2.0 cm)

The fluence rates of 800-nm-emission (Yb-UCNPs) and 540-nm-emission (Nd-UCNPs with different ET efficiency) were simulated at different tumor depths. As shown in Fig. 6(b), the deep (≥2 cm) imaging ability of Nd-UCNPs (Y≥20%) would absolutely beat the Yb-UCNPs. For the shallow layer (≤1 cm) in Fig. 6(b), Yb-UCNPs enable more detectable emission photons than Nd-UCNPs (Y: 10%) since ET efficiency should be considered as the relative low tissue absorption of both two excitations in this region. After calculating the diffusion equation, we find that in Fig. 6(c) the Nd-UCNPs (Y = 13%) with 540-nm-emission could completely replace the Yb-UCNPs with 800-nm-emission for *in vivo* deep imaging. This is the very little ET efficiency and easy to be obtained in many Nd-UCNPs. What's more, this difference were calculated as the ratios of surface UC PL fluence rates between Nd-UCNPs(Y: 13%) and Yb-UCNPs. Surprisingly, we find that the ratio value was 100 at the depth of 1.5 cm, and it enhanced rapidly to about 500 when the depth reached 2.0 cm (Fig. 6(d)). This huge difference may be attributed to the too weak exciting laser power and power-dependent QY for 975 nm laser after much stronger attenuation in deep tissue. Since the ET efficiency has been reported as high as 90% in the Nd-UCNPs [19]. This investigation suggested us that the current Nd-UCNPs are really the powerful tool to replace the Yb-UCNPs for *in vivo* deep imaging, regardless of the effect of Nd^{3+}-Yb^{3+} ET efficiency.

The impact of emission wavelength on the imaging depth. In the deep tissue, both the excitation and emission wavelengths would affect the imaging depth. Nd-UCNPs exhibit the superiority in penetrating excitation due to the diminished tissue absorption of 795 nm light. However, the main energy of most reported Nd-UCNPs UC emission are in the green/blue range [17–21], which may restrict the imaging depth due to its stronger absorption and scattering than the red or the NIR emission [5].

The deep imaging ability of 650 nm (red) and 540 nm (green) emission were investigated in the pork tissue model. The 540 nm emission would decay too quickly to be detected after stronger absorption and scattering, while the 650 nm emission has the lower attenuation (Table 1). At each depth from 0.5 cm to 3 cm, the 650 nm emission has the larger UC PL fluence rate values than that of the 540 nm in Fig. 7(a). The peak fluence rates ratios of 650-nm-emission and 540-nm-emission were calculated at each tumor depth from 0.5 cm to 4.0 cm in Fig. 7(b). The ratio value was about 10 at the depth of 2 cm, and it rapidly increased to 40 at 4-cm-depth. Here this comparison also depend on the signal-to-noise (SNR) ratio of imaging system, and the advantage of red emission may be impaired by the strong noise level. However, UCNP has the unique background-free imaging ability with ultrahigh SNR ratio [3, 10], and the weakest UC signal (10^{-4} W/m^3) in this simulation is strong enough for mostly scientific detectors in the UCNP imaging. Therefore, this investigation showed that the current Nd-UCNPs still need to be optimized

#227211 - $15.00 USD Received 4 Dec 2014; revised 27 Jan 2015; accepted 6 Feb 2015; published 18 Feb 2015

in UC emission wavelength and the remarkable improvement of imaging depth by shifting UC emission from 540 nm (green) to 650 nm (red) is very meaningful and worth to be studied further.

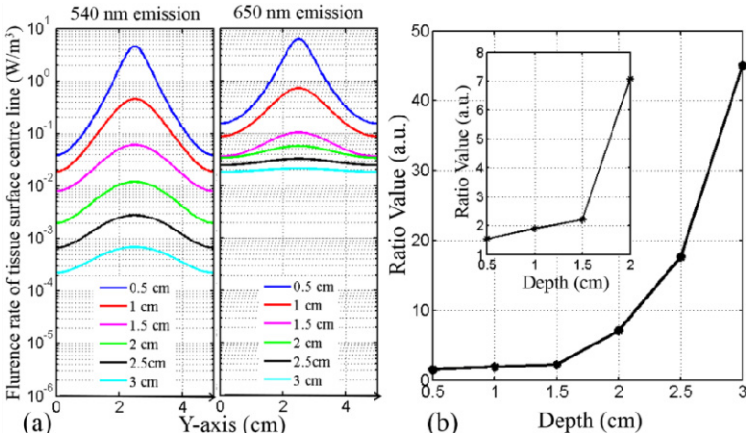

Fig. 7. (a). UC 540 nm (left) and 650 nm (right) emission fluence rate on the tissue surface with tumor located at different depths; (b). peak UC PL fluence rate ratios of 650 nm and 540 nm emission as a function of depth.

4. Conclusion

Several aspects have been investigated computationally and experimentally for high resolution, rapid scanning, deep, and damage-free bioimaging of Nd-UCNPs. For the first time, cell microscopy and three-layer pork tissue were optically modeled to investigate Nd-UCNPs-based bioimaging. Based on two models, the tissue damage index and cells viability were calculated for the 975 nm and 795 nm excitation. The 100% surviving cells and tissue after long-term 795-nm-irradiation have clearly proved that Nd-UCNPs enabled the damage-free imaging *in vitro* and *in vivo* with high power laser irradiation. The experimental results exhibited that high safety power excited Nd-UCNPs enable five times faster scanning microscopy in damage-free microscopy imaging. In addition, with shorter wavelength 795 nm CW laser excitation, Nd-UCNPs provide higher resolution (20% improvement) imaging in multiphoton microscopy, which should not be overlooked in the UCNP application. Two latent factors in deep tissue imaging were firstly proposed and investigated. Calculation results of deep imaging UC process showed that the Nd-UCNPs with relative low 13% Nd^{3+}-Yb^{3+} ET efficiency have already enabled larger imaging depth than Yb-UCNPs. Notably, the ET efficiency has already been managed to the high level (90%) and thus it is an unimportant factor in deep imaging for future Nd-UCNPs development. In addition, simulation results pointed out that the Nd-UCNPs with enhanced 650-nm-emission are recommended for deep tissue bioimaging. This optical investigation will be a meaningful complementary to the Nd-UCNPs research and give a new insight into developing UCNPs-based bio-applications in the future.

Acknowledgments

This work was supported by the Natural Science Foundation of China (61405062), the Guangdong Innovative Research Team Program (201001D0104799318), the Natural Science Foundation of Guangdong province (S2013040014211, S2014060010355), the Postdoctoral Science Foundation of China (2013M530368, 2014T70818) the Discipline and Specialty Construction Fundation of Colleges and Univerisities of Guangdong Province (2013LYM_0017), the Young Faculty Academic Training Foundation of SCNU (2012KJ017).